The Different Nature of the Interdecadal Variability of the Thermohaline Circulation under Mixed and Flux Boundary Conditions

OLIVIER ARZEL, THIERRY HUCK, AND ALAIN COLIN DE VERDIÈRE

Laboratoire de Physique des Océans (UMR 6523 CNRS IFREMER UBO), Brest, France

(Manuscript received 7 July 2004, in final form 30 January 2006)

ABSTRACT

The differences between the interdecadal variability under mixed and constant flux boundary conditions are investigated using a coarse-resolution ocean model in an idealized flat-bottom single-hemisphere basin. Objective features are determined that allow one type of oscillation to be distinguished versus the other. First, by performing a linear stability analysis of the steady state obtained under restoring boundary conditions, it is shown that the interdecadal variability under constant flux and mixed boundary conditions arises, respectively, from the instability of a linear mode around the mean stratification and circulation and from departure from the initial state. Based on the budgets of density variance, it is shown next that the two types of oscillations have different energy sources: Under the constant-flux boundary condition (the thermal mode), the downgradient meridional eddy heat flux in the western boundary current regions sustains interdecadal variability, whereas under mixed boundary conditions (the salinity mode), a positive feedback between convective adjustment and restoring surface heat flux is at the heart of the existence of the decadal oscillation. Furthermore, the positive correlations between temperature and salinity anomalies in the forcing layer are shown to dominate the forcing of density variance. In addition, the vertical structure of perturbations reveals vertical phase lags at different depths in all tracer fields under constant flux, while under mixed boundary conditions only the temperature anomalies show a strong dipolar structure. The authors propose that these differences will allow one to identify which type of oscillation, if any, is at play in the more exhaustive climate models.

1. Introduction

Many observational analyses support the existence of interdecadal variability in the North Atlantic climate system. Based on in situ measurements of temperature and salinity, Levitus (1989) identified a warm salty period in the late 1950s followed by a cold fresh one in the early 1970s: Variations in the Gulf Stream intensity were proposed as an explanation for these long-period changes. Later, Deser and Blackmon (1993) showed that sea surface temperature (SST), sea ice, and fluctuations of the atmosphere in the subpolar gyre evolve synchronously on decadal time scales (8–15 yr). In agreement with the pioneer work of Bjerknes (1964), Kushnir (1994) concluded that the pronounced decadal fluctuations and sea level pressure above subtropical and subpolar gyres in the North Atlantic were an indication of coupled ocean–atmosphere interactions. Hansen and Bezdek (1996) showed evidence that SST anomalies propagating around subtropical and subpolar gyres are well correlated with decadal changes in the North Atlantic Oscillation (NAO). Using hydrographic data, Reverdin et al. (1997) confirmed the propagation of surface-intensified anomalies in the subpolar gyre and suggested that these anomalies were related to fluctuations in slope currents in the Labrador Sea correlated with the NAO. Sutton and Allen (1997) analyzed shipboard observations to indicate downstream propagation of SST anomalies along the North Atlantic Current, with a regular period of 12–14 yr. Similar propagations of SST anomalies, but at a shorter 7.5-yr period, were shown to be part of the pattern exhibiting maximum correlation with the NAO (Da Costa and Colin de Verdière 2002). Delworth and Mann (2000) compared the North Atlantic multidecadal variability simulated in the Geophysical Fluid Dynamics Laboratory (GFDL) coupled model with a reconstruction of climate data over the past few centuries. The simulated climate vari-

Corresponding author address: Olivier Arzel, Institut d'Astronomie et de Géophysique G. Lemaître, Université catholique de Louvain, Chemin du cyclotron, 2, 1348 Louvain-la-Neuve, Belgium.
E-mail: arzel@astr.ucl.ac.be

ability involves fluctuations of North Atlantic thermohaline circulation and is in good agreement with observations. Although the observations are still too sparse to identify the mechanisms that lead to long-term climate change, several mechanisms involving the Atlantic thermohaline circulation (THC) have been proposed to explain such fluctuations.

The strong link between the oceanic poleward heat transport and the thermohaline circulation has motivated several numerical studies with oceanic general circulation models (OGCMs). The interdecadal variability of the thermohaline circulation is very sensitive to air–sea heat and freshwater fluxes, and two types of surface boundary conditions are traditionally used for temperature and salinity. Nudging the surface variables to their climatologies allows one to reconstruct the deep fields but, not surprisingly, this choice leads to steady states. The other alternative is to use flux boundary conditions (as for the wind forcing of the ocean). In this case the underlying assumption is that, whatever happens in the ocean, the atmosphere has constant transports of heat and moisture. Since surface salinity values have no effect on evaporation, some logic is indeed respected. This is obviously more complicated for temperature since a SST anomaly is removed by anomalous heat fluxes on time scales of months to years depending on spatial scales and amplitudes. One way of including this effect is to relax the SST to an imposed atmospheric temperature field. There are two difficulties with this: one is that the sensitivity of heat flux to temperature is not well known and the other is that evaporative fluxes are also expected to depend on SST anomalies. This choice of relaxation of SST and fixed hydrological fluxes, the so-called mixed boundary conditions, has been used for nearly 20 years in ocean modeling, not so much for its demonstrated value but as a first step before adoption of fully coupled ocean–atmosphere models. Obviously the underlying hypothesis of constant air temperature and evaporation/precipitation distribution is easier to accept if the induced ocean variability remains of small amplitude.

Interdecadal oscillations were reproduced in the context of both haline and thermal circulation forced by prescribed fluxes (Huang and Chou 1994; Greatbatch and Zhang 1995). Colin de Verdière and Huck (1999) identified the energy source, or the wave maker, of these oscillations as a baroclinic instability of the western boundary current region, a process later generalized by te Raa and Dijkstra (2002). The name "baroclinic instability" was assigned because of the presence of downgradient eddy heat fluxes in the regions of growth of the oscillations. Under mixed boundary conditions, decadal to interdecadal oscillations had been found earlier (Weaver and Sarachik 1991a,b; Weaver et al. 1991) and an advective mechanism was suggested. Yin and Sarachik (1995) proposed a mechanism of the full cycle involving both advective and convective processes in the subpolar region. The robustness of such oscillations to the coupling with simple atmospheric or thermodynamic ice models was investigated more recently by Huck et al. (2001) and Kravtsov and Ghil (2004).

Several authors have found similarities between interdecadal variability obtained in ocean-only models and more complex coupled models. Chen and Ghil (1996) suggested that the mechanism of variability is the same in an ocean model coupled to an atmospheric energy balance model or forced by mixed boundary conditions Chen and Ghil (1995). Moreover, these authors emphasized the central role of the constant heat flux component in the surface ocean forcing of the coupled model. But under mixed boundary conditions, we shall see that it is the restoring form of the surface heat flux that is crucial to the variability. In contrast with Chen and Ghil (1996), Huck et al. (2001) found that the interdecadal variability that emerges in an idealized ocean-only model forced by fixed surface heat flux persists when coupled to a simple atmospheric energy balance model. Greatbatch and Zhang (1995) suggested that their oscillations (period of 50 yr) obtained in an ocean-only model forced by a constant, zonally uniform, surface heat flux have many similarities with the ones found in the GFDL coupled ocean–atmosphere model (Delworth et al. 1993).

The purpose of this study is then to determine some objective features allowing one to distinguish the variability under mixed boundary conditions and flux boundary conditions. After examining the transient behavior of the circulation from steady conditions toward interdecadal variability, we will compare the spatial and temporal structure of density perturbations during an oscillation cycle and explore the mechanisms through which these perturbations can maintain themselves against all damping processes. We will show that the mechanisms involved in the interdecadal variability under both the mixed and flux boundary conditions differ fundamentally.

The outline of this work is as follows. In section 2, the ocean model is briefly described; the various experiments under relaxation, flux, and mixed boundary conditions are presented in section 3. The structure and propagation of the perturbations for the two surface boundary conditions are investigated in section 4. The energy sources of the two types of thermohaline circulation variability are analyzed in section 5 using the

density variance budget. Section 6 summarizes and concludes our study.

2. The ocean model

Our interest is in the description of the differences of modes of variability of ocean models running under mixed and constant flux boundary conditions at interdecadal time scales. We thus choose the simplest three-dimensional ocean model capable of representing the thermohaline circulation and its associated poleward heat transport. Integrations of several thousand years are required, so a coarse-resolution ocean model is employed. The variability produced by such models involves long time-scale processes compared to the inertial period so that the momentum equations become diagnostic. In this planetary geostrophic limit there is no production of mesoscale eddies. The model is the same as in Colin de Verdière and Huck (1999) and Huck et al. (1999b), based on the planetary geostrophic (hydrostatic and Boussinesq) equations in spherical coordinates, which is well suited to the study of extratropical large-scale flows (Salmon 1986; Colin de Verdière 1988; Winton and Sarachik 1993),

$$f\mathbf{k} \times \mathbf{u} = -\rho_0^{-1}\boldsymbol{\nabla}_h p + a_h \nabla_h^2 \mathbf{u}, \tag{1}$$

$$\partial_z p = -\rho g, \tag{2}$$

$$\boldsymbol{\nabla}_h \cdot \mathbf{u} + \partial_z w = 0, \tag{3}$$

$$\partial_t T + \mathbf{u} \cdot \boldsymbol{\nabla} T = k_h \nabla_H^2 T + k_v \partial_z^2 T + F_T + C_T, \tag{4}$$

$$\partial_t S + \mathbf{u} \cdot \boldsymbol{\nabla} S = k_h \nabla_H^2 S + k_v \partial_z^2 S + F_S + C_S, \tag{5}$$

and

$$\rho = \rho_0(1 - \alpha T + \beta S), \tag{6}$$

where f is the Coriolis parameter, $\mathbf{u}(w)$ is the horizontal (vertical) velocity field, p is the pressure, ρ is the density, T is the temperature, S is the salinity, and $\mathbf{k}$ is the unit vector upward in the vertical direction; C_T and C_S represent the changes in temperature and salinity due to the convective adjustment that ensures static stability of the water column, F_T and F_S are the air–sea flux of temperature and salt applied to the mixed layer (h_s),

$$F_T = \tau_T^{-1}(T_R - T)$$

and

$$F_S = \tau_s^{-1}(S_R - S),$$

for restoring boundary conditions and

$$F_T = (\rho_0 C_{pw} h_s)^{-1} Q$$

and

$$F_S = -S_0(P - E)/h_s$$

TABLE 1. Standard values of the model parameters.

S_0	35 psu	Reference salinity
C_{pw}	4000 J K^{-1} kg^{-1}	Seawater heat capacity
ρ_0	1000 kg m^{-3}	Reference seawater density
α	1.5×10^{-4} K^{-1}	Thermal expansion coefficient
β	8×10^{-4} psu^{-1}	Haline expansion coefficient
k_v	10^{-4} m^2 s^{-1}	Vertical diffusivity
a_h	10^5 m^2 s^{-1}	Horizontal Laplacian viscosity
k_h	10^3 m^2 s^{-1}	Horizontal diffusivity
τ_T	66 days	Restoring time scale for SST
τ_S	30 days	Restoring time scale for SSS

for prescribed surface flux, where T_R, S_R, Q, and $P - E$ are the restoring temperature and salinity fields and the prescribed surface heat and freshwater fluxes, respectively. The numerical values of the model parameters are listed in Table 1. Sensitivity studies have revealed that interdecadal variability emerges for vertical mixing larger than 5×10^{-5} m^2 s^{-1} under both mixed and flux boundary conditions, but disappears for values of about 10^{-5} m^2 s^{-1}. The vertical mixing k_v is therefore arbitrarily fixed to 10^{-4} m^2 s^{-1} in the present study, as in Weaver et al. (1993), for example. This diffusivity is about an order of magnitude larger than in situ measurements carried out away from topography (Ledwell et al. 1993), but agrees with values inferred from the large-scale abyssal stratification (Munk 1966). Munk and Wunsch (1998) emphasized that a vertical mixing of about 10^{-4} m^2 s^{-1} is still needed in small source regions of buoyancy flux from which the water masses are exported into the ocean exterior. Our vertical mixing is thus assumed to represent the large-scale diapycnal diffusivity. The domain is a flat-bottomed sector of a sphere, with dimensions appropriate for the North Atlantic (64° in longitude from 10° to 66°N). Lateral boundaries are solid vertical walls where no-slip and no-flux boundary conditions are applied. We concentrate only on the response of the baroclinic flow to changes in surface boundary conditions; thus, no wind forcing is considered in our study (hence, there is no barotropic flow given the flat bottom and the absence of bottom friction). The model is run at a coarse horizontal resolution of 2° with vertical grid spacing increasing from 50 m (h_s) at the surface to 550 m at the bottom (15 levels, 4500 m deep). A linear equation of state is used in order to isolate more easily the sources and sinks of density variance.

3. The experiments

Because of the absence of feedback between sea surface salinity (SSS) and freshwater flux, some authors argue that the boundary conditions in a coupled ocean–

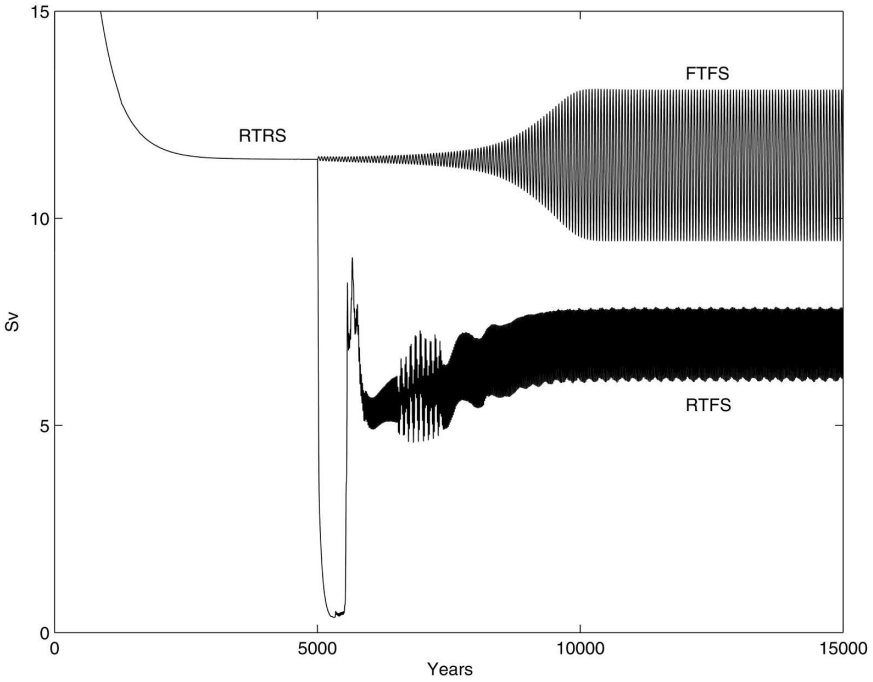

FIG. 1. Maximum meridional overturning streamfunction (Sv) for the ocean model running under restoring boundary conditions (RTRS) until year 5000. Mixed boundary conditions (RTFS) and constant flux (heat and freshwater) boundary conditions are applied at year 5000 of the integration.

atmosphere system are similar to mixed boundary conditions in an ocean-only model (Weaver et al. 1991). Many others have considered instead that the ocean sees almost a constant surface heat flux (Greatbatch and Zhang 1995; Colin de Verdière and Huck 1999). To find equivalent behavior (if any) in the coupled system, we must qualify the differences in the interdecadal variability obtained under both mixed and flux boundary conditions. To do this, we use the same steady-state thermohaline circulation obtained under restoring boundary conditions as the initial state of experiments under both mixed and flux boundary conditions.

The ocean model is spun up using restoring boundary conditions (Haney 1971) for both temperature and salinity (experiment RTRS, R indicating "Restoring") from an ocean at rest with uniform temperature (4°C) and salinity (35 psu). SST is restored toward a prescribed temperature distribution function of latitude as a half-wavelength cosine profile from 25°C at 10°N to 0°C at 66°N and salinity toward a linear profile from 37 psu at 10°N to 35.5 psu at 66°N.

When a steady state is reached, surface heat and salinity fluxes are diagnosed and used for further experiments under flux (F) boundary conditions for both temperature and salinity (experiment FTFS, F indicating "flux") and mixed boundary conditions (experiment RTFS, restoring for temperature and constant flux for salinity). Note that a large ensemble of simulations has been performed in order to find variability under mixed and flux boundary conditions with the same initial steady state obtained at the end of the restoring experiment.

The thermal exchange coefficient λ is fixed to 35 W m^{-2} K^{-1}, reproducing a realistic restoring time scale of approximately 2 months for the uppermost level thickness of 50 m of the model. Although there is no physical reason to use a different value for the salinity restoring time scale, we purposely chose a smaller restoring time scale of 30 days in order to trigger oscillations under mixed boundary conditions. Tziperman et al. (1994) have shown that increasing the restoring time scales for salinity in the restoring experiment results in a weaker freshwater forcing. This makes the transition from restoring to mixed boundary conditions stable, instead of undergoing the well-known polar halocline catastrophe (Bryan 1986). Mikolajewicz and Maier-Reimer (1990) used a 40-day restoring time scale for SSS. For values larger than this the transition to mixed boundary conditions was stable in our configuration.

The maximum overturning circulation (Fig. 1) under constant heat and freshwater fluxes slowly evolves into a limit cycle over approximately 5000 years, the period

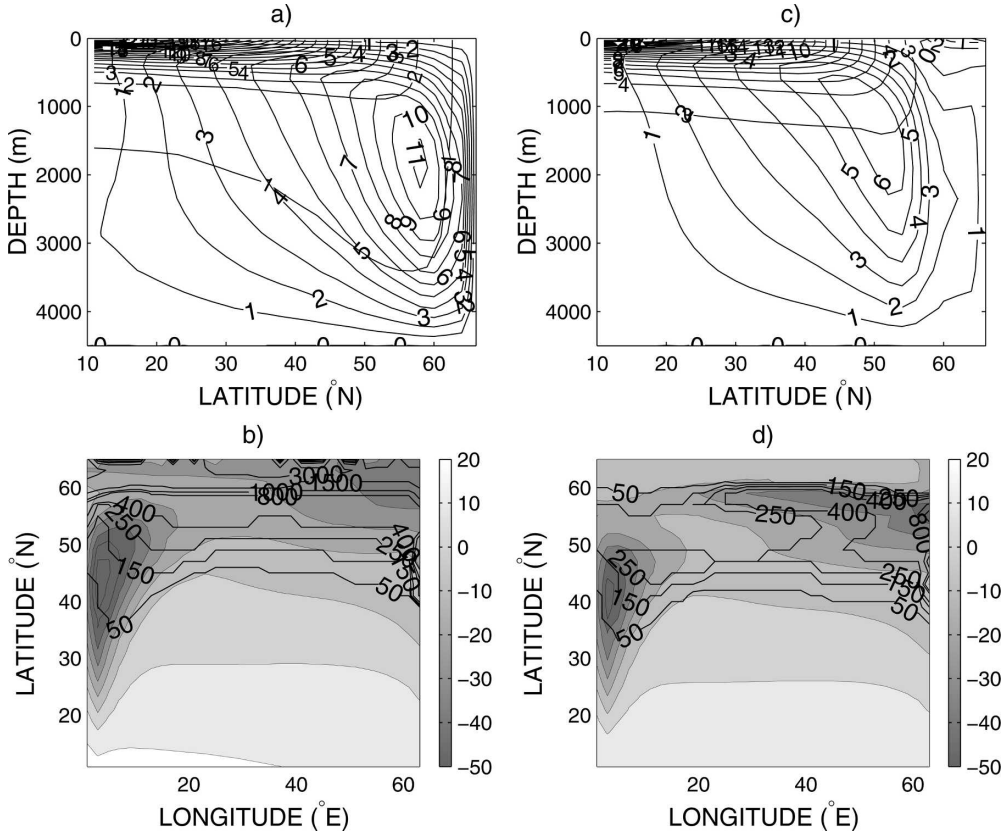

FIG. 2. The mean state of the (a), (b) FTFS and (c), (d) RTFS experiments: (a), (c) meridional streamfunction (Sv) and zonally averaged temperature fields contours (°C) and (b), (d) surface heat flux (W m^{-2}) and convection depth (m).

of which is about 57 yr. The overturning fluctuates around a time-mean state (11.4 ± 1.3 Sv; Sv ≡ 10^6 m^3 s^{-1}) that is very close to the steady state obtained in the restoring experiment. The time-averaged meridional streamfunction is clearly a thermally driven cell (Fig. 2a): Deep-water formation occurs mainly along the northern boundary where convection reaches the bottom layers of the basin (Fig. 2b). The steady-state thermohaline circulation obtained under restoring boundary conditions is also unstable upon the transition to mixed boundary conditions; the circulation undergoes a polar halocline catastrophe followed by a flush event associated with the restart of convective activity (Bryan 1986; Weaver and Sarachik 1991a; Winton and Sarachik 1993; Wright and Stocker 1991). Further along, the model settles into perpetual oscillations, with a period of 19.2 yr, more than a factor of 2 shorter than in FTFS. The time-averaged meridional overturning of RTFS is illustrated in Fig. 2c. Deep-water formation takes place farther away from the northern boundary, around 50°N, because of the existence of a halocline with a low surface salinity (34 psu) caused by large precipitation rates (150 cm yr^{-1}). The convection depth (Fig. 2d) is also weaker (maximum of 400-m depth) than in FTFS. The time-averaged model state is then obviously different from the initial state and this is mostly due to changes in the region of deep-water formation.

By performing a linear stability analysis of the steady state obtained under restoring boundary conditions, Huck and Vallis (2001) demonstrated that the interdecadal oscillation obtained under prescribed heat flux forcing arise from an unstable linear mode of the mean stratification and circulation in their idealized flat-bottom ocean model. We perform here the same analysis, using the same model and empirical linearization method, for the steady state of RTRS. It appears that the interdecadal oscillations driven by constant surface heat and freshwater fluxes arise similarly through the growth of an unstable linear mode. However, the growth time period of this mode is 1136 yr, to be compared with the 56 yr for the purely thermally driven case (Huck and Vallis 2001).

The same linear stability analysis carried out under

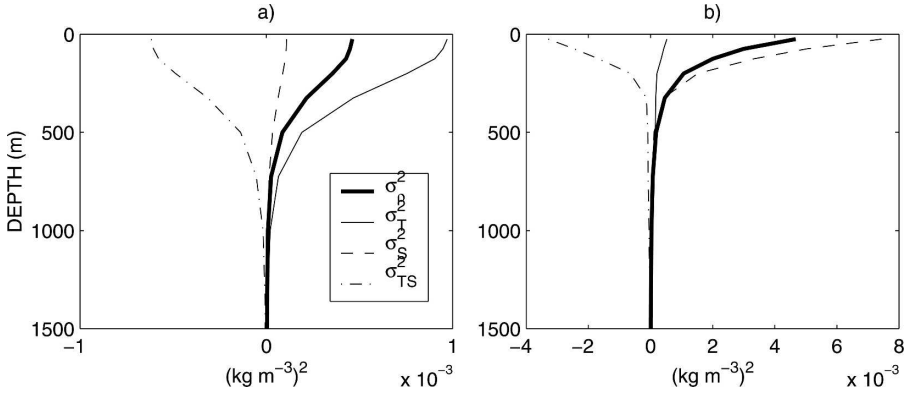

FIG. 3. Horizontal basin-averaged perturbation density variance as a function of depth in term of temperature and salinity under (a) flux (FTFS) and (b) mixed boundary condition (RTFS). The legend indicates variance of density perturbation σ_ρ^2, owing to temperature $\sigma_T^2 = \langle\overline{\alpha^2 T'^2}\rangle$, salinity $\sigma_S^2 = \langle\overline{\beta^2 S'^2}\rangle$, and temperature–salinity correlations $\sigma_{TS}^2 = -2\langle\overline{\alpha\beta T'^2 S'^2}\rangle$.

mixed boundary conditions has not revealed an unstable mode, suggesting a different character of the oscillations. Indeed, Huck and Vallis (2001) have shown that restoring boundary conditions suppress the large-scale baroclinic instability mechanism (Colin de Verdière 1986) that is responsible for the variability under prescribed surface heat flux since the instability growth rate is smaller than the damping rate associated with the surface restoring.

4. Structure of the perturbations

Although the interdecadal variability obtained in the purely oceanic models with constant air–sea fluxes (Greatbatch and Zhang 1995; Colin de Verdière and Huck 1999) or mixed boundary conditions (Weaver et al. 1991; Chen and Ghil 1995) have both been analyzed, a specific comparison of the spatial and temporal structure of the perturbations has not been performed yet. Therefore, we propose to compare the propagation of the perturbations across the basin and their vertical structure under mixed and constant flux boundary conditions.

The first obvious difference lies in the dependence of density perturbations upon salinity and temperature anomalies (Fig. 3). When mixed boundary conditions are used, surface temperature is strongly constrained by the restoring surface heat flux and remains relatively close to the restoring temperature field, whereas salinity variations are not so restricted. Density perturbations are then essentially salinity driven. Nevertheless, we will show in section 5 that the temperature influence remains crucial for sustaining the oscillation through the restoring surface heat flux. In contrast, the variability under constant surface fluxes is essentially thermally driven, the salinity reducing the oscillation amplitude.

The description of the spatial structure of the surface-intensified temperature anomalies that emerge under constant heat flux boundary conditions has been provided in Colin de Verdière and Huck (1999). In the western third of the basin, large amplitude anomalies remain stationary with no propagation, while in the interior, weaker amplitude perturbations propagate westward within a broad latitude band (40°–55°N). These are planetary Rossby waves modified by the mean eastward surface zonal flow and mean meridional density gradient. However, their propagation against the mean current is not always observed. The same behavior appears here when a constant freshwater flux is added (Figs. 4a–c), but with a propagation time across the basin two times as long (see also Greatbatch and Zhang 1995). The salinity decreases the mean meridional density gradient on which the perturbations propagate and, according to Colin de Verdière and Huck (1999), this further decreases the westward phase velocity of temperature-dominated density anomalies and, hence, increases the oscillation period. This agrees with Huck et al. (2001) who showed that the period scales roughly as L_x/U, where L_x is the longitudinal extent of the basin and U is the geostrophic velocity scale in the thermocline.

Inspection of characteristic phase diagrams in the $z - t$ plane (Figs. 5a–b) reveal that the temperature and salinity anomalies are highly correlated at all depths from the surface to 800 m, in good agreement with Greatbatch and Zhang (1995). The salinity acts to reduce the magnitude of the temperature-dominated density anomalies and consequently reduces the magnitude of the oscillations. The vertical structure shows upper-level anomalies leading deeper anomalies (below 300 m) by one-quarter period, in agreement with Colin de Ver-

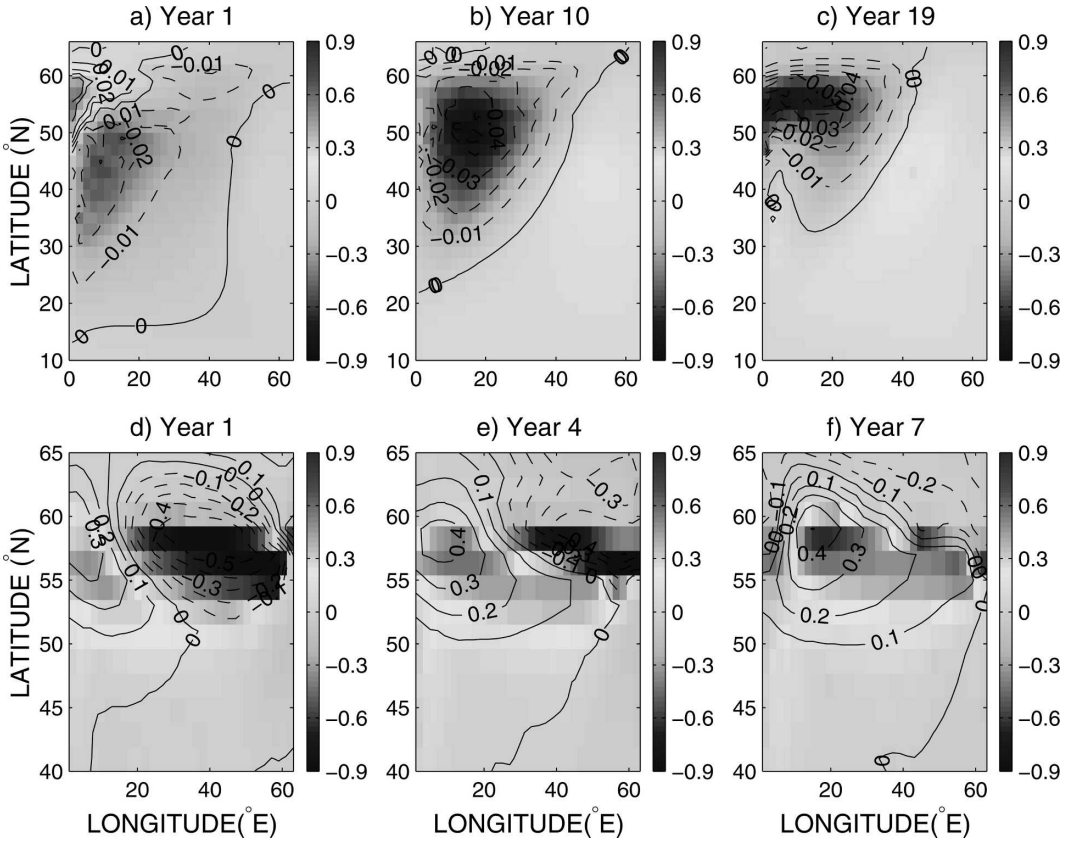

FIG. 4. SST (grayscale; °C) and SSS anomalies (contours; psu) during a half oscillation cycle under (a)–(c) flux and (d)–(f) mixed boundary conditions. The latitudinal scale is expanded in the region where perturbations propagate eastward [in panels (d)–(f)]. The other half cycle is similar for the two boundary conditions but with perturbations of opposite sign.

dière and Huck (1999). Such vertical phase lags are well known to be necessary to produce eddy heat flux for nearly geostrophic flows. This strongly suggests that the basic driving mechanism for the FTFS interdecadal oscillations is the same as under a single component flux, that is, a regional baroclinic instability in the vicinity of the western boundary.

Let us contrast the situation under mixed boundary conditions, where the perturbations are seen to emerge in a region of net evaporation (59°N) close to the western boundary (Weaver and Sarachik 1991a,b; Weaver et al. 1993). The perturbations propagate northeastward at northern latitudes, more precisely in regions where deep-water formation takes place between 50° and 60°N (Figs. 4d–f). Once they reach the northeastern corner, they are almost erased by the convective adjustment. From there, they return quickly westward in about 2 yr along the northern boundary. The vertical structure of all tracer fields at a point located in the most unstable region in the eastern half of the basin (59°N, 40°E) is shown in Figs. 5c–d. An interesting difference from FTFS is that the temperature and salinity anomalies are positively correlated near the surface (0–300-m depth) and negatively correlated below. As shown by a detailed analysis of the anomalous heat and salt balance, only the surface thermal boundary condition and the convective adjustment can explain such a distribution since the advective and diffusive processes act in the same way for temperature and salinity anomalies. In the surface mixed layer, temperature anomalies are subjected to thermal damping and, for this reason, they do not penetrate much beyond 300-m depth, while the salinity anomalies, free of surface restoring boundary conditions, extend more deeply.

We now investigate the processes responsible for this interesting vertical organization of perturbations under mixed boundary conditions. When the surface density anomaly is positive (SST′ and SSS′ both positive), the column is unstable and the subsequent convective adjustment brings warm salty waters upward and cold freshwater downward since both temperature and salinity increase with depth; the salinity and temperature

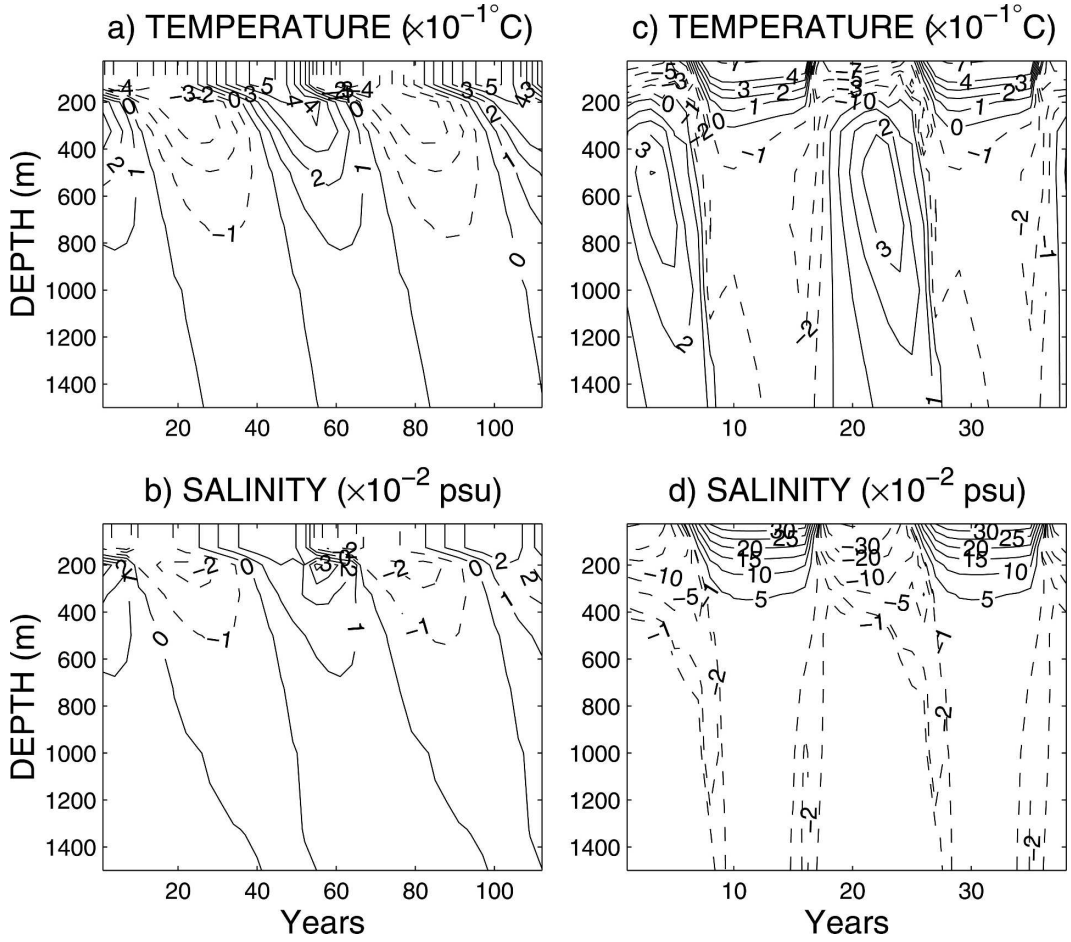

FIG. 5. Characteristic diagrams of the temperature and salinity anomalies in the z–t plane in the most unstable region for experiments under constant air–sea forcing [(a), (b) expt FTFS at 49°N, 10°E] and under mixed boundary conditions [(c), (d) expt RTFS at 59°N, 39°E].

changes due to anomalous convection are positive near the surface and negative at lower levels. Hence, a cold temperature anomaly appears below the anomalous warm surface waters. The effect also decreases the salinity anomaly at lower levels, but the decrease is not strong enough to generate negative salinity anomalies at these depths. The argument is similar when a negative density anomaly (SST′ and SSS′ both negative) is present near the surface. In this case, the column is stable and no convective motions are triggered, but the anomalous convection, opposite to the time-averaged convection, brings cold freshwater upward and warm salty waters downward. The result is a positive temperature anomaly that appears below the anomalous cold surface waters, with a magnitude (0.3°C) greater than the negative ones (−0.1°C) at the same levels (Fig. 5c). Negative salinity anomalies are also shallower than the positive ones (500 vs 1000 m, Fig. 5d). The asymmetry between the amplitudes (and e-folding depths for salinity) of the positive and negative temperature and salinity anomalies is due to the differences of temperature and salinity changes caused by the anomalous convective adjustment when the column is either stable or unstable. To summarize, the temperature anomalies are characterized by a dipolar structure, while the salinity anomalies are preferentially surface intensified.

5. The density variance budget

Interdecadal variability has now been widely observed both in midlatitude ocean basins and in various numerical ocean models, yet the identification of the sources of the variability remains obscure. If some authors advocate that the only serious contender is the time-varying air–sea forcing, idealized studies have shown that variability can arise under *constant* air–sea fluxes.

To clarify this issue of the sources of the variability, we need first to agree on an objective measure of the strength of the variability. Observationally, the simplest measure is the temperature variance supplemented whenever possible by the salinity variance, the statistics being carried out through a combination of temporal and spatial averaging. If the temperature and salinity are positively correlated in a way to give zero contribution to density variance, we are witnessing a passive evolution of temperature and salinity whose origins can be traced back to peculiar combinations of temperature and salinity forcings and/or to the effect of lateral mixing along density surfaces (Stern 1967). Focusing on *T*/*S* variability that can feedback on the circulation itself, the measure that imposes itself is the density (or buoyancy) variance. Several studies have used the evolution equation of this variance, with success, to identify the sources of the variability under various climatic processes [Welander (1982) for mixed boundary conditions, Colin de Verdière and Huck (1999) for flux boundary conditions, Colin de Verdière and Blanc (2001) in a coupled ocean–atmosphere model]. In the context of the present analysis, we assume a linear equation of state. The approach that we develop will need to be expanded to take into account the case for which the variability is clearly associated with the nonlinearity of the equation of state Pierce et al. (1995).

With the internal energy equation governing the temperature and salinity evolution, the perturbation equation for nondimensional density $\rho' = -\alpha T' + \beta S'$ can be written as

$$\partial_t \rho' + \bar{\mathbf{u}} \cdot \boldsymbol{\nabla} \rho' + \mathbf{u}' \cdot \boldsymbol{\nabla} \bar{\rho} = D' + B', \tag{7}$$

where D' combines the sum of the subgrid-scale diffusive and convective operators and B' represents the net perturbation density forcing due to the sum of the salinity and temperature surface fluxes ($\beta F_s' - \alpha F_T'$) distributed over a mixed layer of constant depth. The mean state, noted by an overbar can be either a suitable time average or a reference state at equilibrium. The two are not equivalent since "turbulent fluxes" can influence the mean state in the former case, but this should not create difficulties as we only require that the mean velocity be divergenceless. If we multiply (7) by ρ' and average temporally and spatially over the domain of interest, we obtain

$$\frac{1}{2}\partial_t \langle \overline{\rho'^2} \rangle = -\langle \overline{\mathbf{u}'\rho'} . \nabla \bar{\rho} \rangle + \langle \overline{\rho' B'} \rangle + \langle \overline{\rho' D'} \rangle, \tag{8}$$

where the overbar and the angle brackets denote a time average over one oscillation period and a spatial average, respectively. Of the three terms on the rhs of (8), the last is strictly nonpositive and represents the diffusive sink of density variance. Only the first two can generate the variability. The first is, indeed, positive if the eddy fluxes are oriented down the mean density gradient. This term is familiar from baroclinic instability theory when the horizontal part of the density fluxes dominates, and transfer of potential energy from the mean to the perturbation is associated with the instability. In the quasigeostrophic context, the density variance is proportional to the available potential energy as defined by Lorenz (1955). This term has been pinpointed by Colin de Verdière and Huck (1999) as the source of the variability in the constant flux experiments for which the second term $\langle \overline{\rho' B'} \rangle$ vanishes. The novel situation is when the surface boundary conditions are mixed in which case the forcing term reduces to

$$\langle \overline{\rho' B'} \rangle = -\alpha^2 \lambda \langle \overline{T'^2} \rangle + \alpha\beta\lambda \langle \overline{T'S'} \rangle, \tag{9}$$

where these quantities are calculated in the forcing layer only. For this term to be a source, the temperature and salinity in the mixed layer must be sufficiently well positively correlated for the second term to exceed the first in (9). By introducing the density ratio in the mixed layer

$$R_\rho = \frac{\alpha \langle \overline{T'^2} \rangle^{1/2}}{\beta \langle \overline{S'^2} \rangle^{1/2}}, \tag{10}$$

and the correlation coefficient between temperature and salinity

$$C_{TS} = \frac{\langle \overline{T'S'} \rangle}{\langle \overline{T'^2} \rangle^{1/2} \langle \overline{S'^2} \rangle^{1/2}}. \tag{11}$$

Equation (9) becomes

$$\langle \overline{\rho' B'} \rangle = \alpha\beta\lambda \langle \overline{T'^2} \rangle^{1/2} \langle \overline{S'^2} \rangle^{1/2} [C_{TS} - R_\rho]. \tag{12}$$

This last expression shows that, for the air–sea forcings to generate variability under mixed boundary conditions, the density ratio must be less than one (the salinity perturbation dominates) and the temperature–salinity correlation coefficient must be positive and large enough to exceed the density ratio. As we show next, the flux experiments and the mixed boundary conditions experiments have completely different source terms in the density variance budget [(8)], and, therefore, can be said to be of a different nature.

a. Flux boundary conditions

The downgradient meridional eddy temperature fluxes ($-\overline{v'T'}\partial_y \bar{T}$) provide the source of density variance under constant air–sea forcing (FTFS), and the terms containing zonal and vertical velocities are positive but negligible relative to the meridional term (Table 2).

TABLE 2. Contributions to the density variance budget under mixed (RTFS) and flux (FTFS) boundary conditions in 10^{-12} yr^{-1}. In both case the convective adjustment decreases the density variance and stabilizes the flow, just like vertical mixing. The Heaviside step function $\Gamma(z)$ is 1 in the mixed layer and 0 elsewhere.

Expt	FTFS	RTFS
$-\langle\overline{u'\rho'}\partial_x\overline{\rho}\rangle$	0.17	1.71
$-\alpha^2\langle\overline{v'T'}\partial_y\overline{T}\rangle$	6.76	8.07
$-\beta^2\langle\overline{v'S'}\partial_y\overline{S}\rangle$	0.46	17.82
$\alpha\beta\langle\overline{v'T'}\partial_y\overline{S}\rangle$	−1.76	−8.27
$\alpha\beta\langle\overline{v'S'}\partial_y\overline{T}\rangle$	−1.57	−16.80
$-\langle\overline{v'\rho'}\partial_y\overline{\rho}\rangle$	3.89	0.82
$-\langle\overline{w'\rho'}\partial_z\overline{\rho}\rangle$	0.88	3.24
$\alpha^2\langle\overline{T'C'_T}\rangle$	1.70	41.61
$\beta^2\langle\overline{S'C'_S}\rangle$	2.67	33.89
$-\alpha\beta\langle\overline{T'C'_S}\rangle$	−3.72	−14.56
$-\alpha\beta\langle\overline{S'C'_T}\rangle$	−1.24	−98.00
$\langle\overline{\rho'C'_\rho}\rangle$	−0.59	−37.06
$-\alpha^2\lambda\langle\Gamma(z)\overline{T'^2}\rangle$	0	−32.30
$\alpha\beta\lambda\langle\Gamma(z)\overline{T'S'}\rangle$	0	100.98
$\alpha\lambda\langle\Gamma(z)\overline{\rho'T'}\rangle$	0	68.68

The largest positive values (corresponding to the most unstable region) appear in the northern third of the western boundary region (Fig. 6a), and the positive eddy temperature fluxes at this location appear to be at the heart of the existence of the oscillation as in Colin de Verdière and Huck (1999) and te Raa and Dijkstra (2002). In the interior, the perturbed temperature fluxes ($\overline{v'T'}$) are mainly negative, resulting in a stabilization of the flow.

The linear stability analysis carried out in section 3 has revealed marked differences in the growth time scale of perturbations between the variability with fixed surface heat and freshwater fluxes and the variability with constant surface heat but zero freshwater flux. Indeed, the influence of salinity on the variability is twofold. This includes first a decrease of the mean meridional density contrast. The strength of mean flow as well as the mean vertical shear, which is the source of instability, is then reduced. Second, it decreases the magnitude of density anomalies that are temperature driven. These two effects together make the driving term of density variance ($-\overline{v'T'}\partial_y\overline{T}$) smaller under constant surface heat and freshwater fluxes than under constant surface heat and zero freshwater fluxes. This results in a smaller growth rate of density variance in the former case than in the second and therefore explains the differences highlighted by the linear stability analysis.

b. Mixed boundary conditions

In contrast to experiments with constant air–sea fluxes, the density variance owing to the interaction between eddy density fluxes and mean density gradient appears negligible. The source term $\rho' B'$ is now the driving term of density variance tendency (Table 2). However, it does not allow by itself to provide a clear

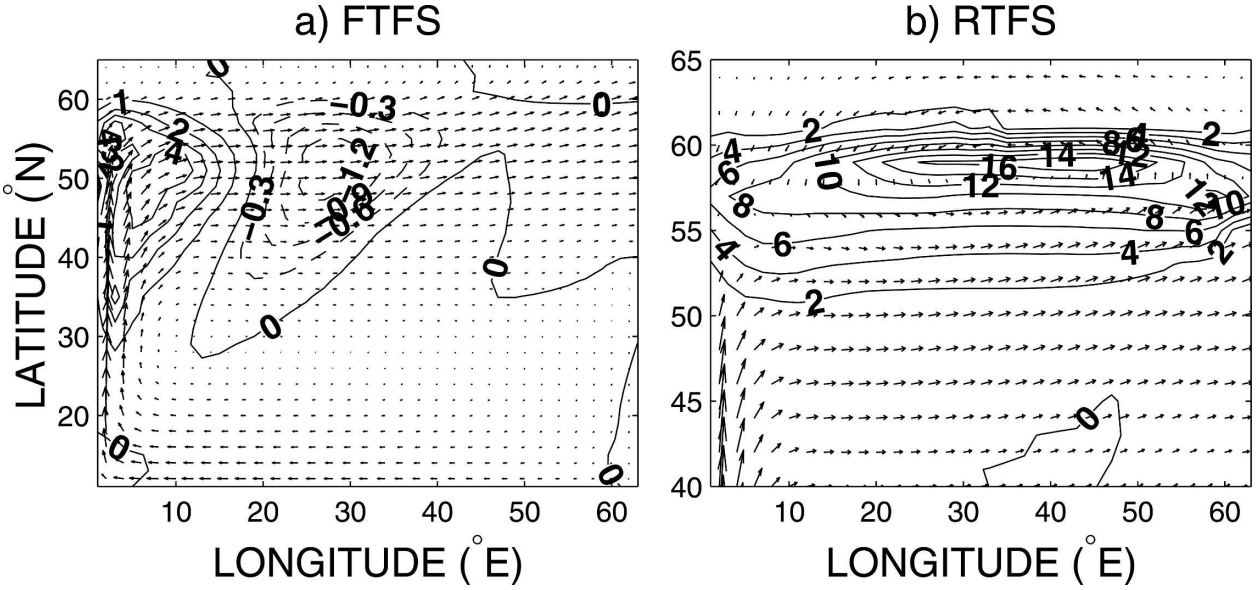

FIG. 6. The driving term of density variance under (a) flux boundary conditions [$\rho_0^2\alpha^2\overline{v'T'}\partial_y\overline{T}$, $\times 10^{-3}$ (kg m^{-3})^2 yr^{-1}]; (b) mixed boundary conditions, strictly nonzero in the forcing layer only [$\rho_0^2\alpha\beta\lambda\overline{T'S'}$, $\times 10^{-2}$ (kg m^{-3})^2 yr^{-1}]. Note the expanded latitudinal scale in the region where perturbations propagate eastward. For both boundary conditions, the mean surface current averaged in the upper 250 m is superimposed.

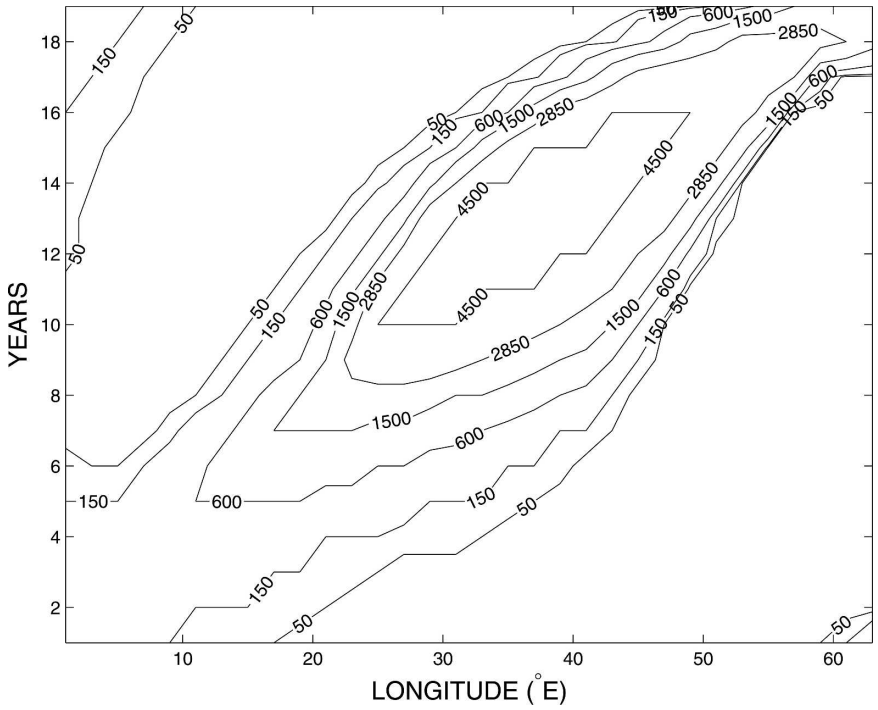

FIG. 7. Phase diagram of convection depth (m) as a function of longitude and time at 59°N. The convection depth increases eastward and reaches the bottom (4500 m) around the middle of the basin.

understanding of the mechanism responsible for the growth or maintenance of perturbations against dissipation. To address this question, some additional developments are required and we investigate further the density variance budget in order to provide a plausible explanation for the origin of the positive feedback involving the air–sea forcing.

As we have demonstrated before, this source term means that the haline forcing dominates the thermal forcing (salinity anomalies control the density anomalies) and that the correlation between SST and SSS anomalies is positive and exceeds the perturbation density ratio. This is what we observe: C_{TS} always exceeds the perturbation density ratio R_ρ in the region of interest (0.9 vs 0.25, respectively).

The spatial structure of the term that dominates the growth of density variance $\alpha\beta\lambda(\overline{T'S'})$, the positive part in $\overline{\rho' B'}$, is shown in Fig. 6b: the largest positive values appear in the middle of the basin. Note that this region does not coincide with the location where the density perturbations emerge (close to the western boundary around 59°N in the localized area of net evaporation) but, instead, coincide with the region where convection is the deepest (Fig. 7): This indicates that the convective adjustment might be important in the process generating the variability.

The basic interpretation of the positive feedback $\rho' B'$ can be viewed as follows: let us suppose that the surface density anomaly is positive ($\rho' > 0$, $T' > 0$, $S' > 0$); then the anomalous surface cooling reinforces the initial density perturbation ($\alpha\lambda T' > 0$). As a result, the density variance increases because $-\alpha^2\lambda T'^2 + \alpha\beta\lambda T'S'$ is positive. In the same manner, if the initial surface density anomaly is negative ($\rho' < 0$, $T' < 0$, $S' < 0$), then the anomalous surface heating reinforces the initial density perturbation ($\alpha\lambda T' > 0$), and again the density variance increases.

Because of the thermal damping of SST anomalies through the restoring boundary condition, the anomalous air–sea forcing B' would be expected to decrease along with the magnitude of the source term $\rho' B'$ during the whole propagation of perturbations, but, as noted previously, the magnitude of the source term increases eastward and is maximum around the middle of the domain. Thus, an additional process must necessarily exist, allowing the SST anomalies to maintain themselves against thermal damping. Table 2 indicates that temperature and salinity anomalies are enhanced through the convective adjustment since temperature and salinity variance tendencies related to convection are both positive ($\alpha^2\langle\overline{T'C'_T}\rangle$ and $\beta^2\langle\overline{S'C'_S}\rangle$). Moreover, these variance tendencies are intensified in the upper

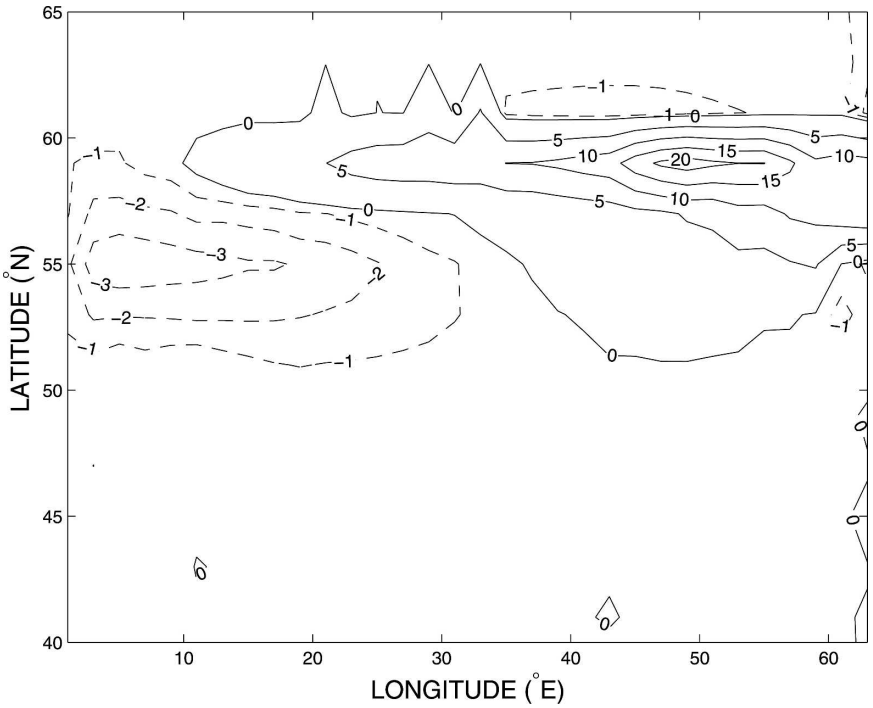

FIG. 8. Sum of temperature variance tendencies in the forcing layer related to anomalous restoring surface heat flux and to convective adjustment [$\rho_0^2\alpha^2(-\lambda\overline{T'^2} + \overline{T'C'_T})$, $\times 10^{-3}$ (kg m^{-3})^2 yr^{-1}].

ocean. This is possible because both temperature and salinity increase with depth in the region of propagation of the perturbations since the net precipitation rate (-10 cm yr^{-1}) and the cooling surface heat flux in these latitudes produce surface waters colder and fresher than deeper waters. Thus, when the surface density anomaly is positive (again when SST and SSS anomalies are both positive), the water column is unstable and the anomalous convection brings warm and salty waters upward: the result is an enhancement of SST and SSS anomalies associated with a damping of surface density anomalies. On the other hand, when the surface density anomaly is negative (SST and SSS anomalies are both negative), the water column is stable and no convective adjustment is triggered. SST and SSS changes owing to anomalous convection are then opposite to those related to the convection averaged over one oscillation period, and cold and fresh waters are brought upward. The result is again an enhancement of SST and SSS anomalies with a damping of surface density anomalies in order to ensure the final stability of the water column.

We can now describe the overall positive feedback responsible for the existence of variability under mixed boundary conditions. Suppose that a surface-intensified density anomaly emerges in the localized evaporation region close to the western boundary. Independent of the sign of the density perturbation, the corresponding SST and SSS anomalies are enhanced through convective adjustment during their eastward propagation across the basin because $T'C'_T$ and $S'C'_S$ are both positive in the mixed layer and the sea surface density perturbation is damped ($\rho'C'_\rho < 0$). Thus, a competition arises for the SST anomaly between the amplification through convective motions and thermal damping. To maintain the SST anomalies against thermal damping and dissipation, we conclude that the subsequent damping of SST anomalies through restoring surface heat flux must necessarily be smaller than the amplification through convective adjustment and $(-\lambda T'^2 + T'C'_T)$ must be positive in the mixed layer. A confirmation is provided in Fig. 8 where, except in the western part of the domain, the amplification of SST anomalies through anomalous convection dominates the anomalous thermal damping, and increases eastward, allowing the SST and SSS anomalies to maintain themselves against dissipation. Moreover, note that convection is responsible for the strong correlations between SST and SSS anomalies to finally exceed the perturbation density ratio in (12). For the case of a positive density anomaly, this results in a continuous increase of the convection depth during the eastward propagation of

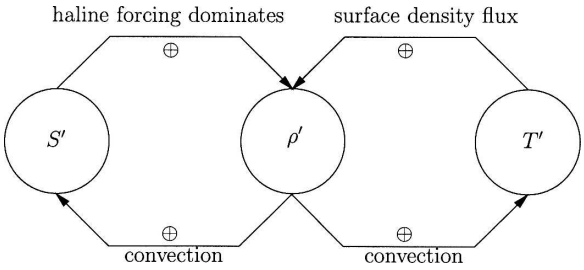

FIG. 9. Schematic view of the positive convective surface heat flux feedback responsible for the growth of density variance under mixed boundary conditions. The symbol ⊕ denotes a growth of anomalies. The feedback involves a (left) rapid salinity feedback and (right) a slow temperature feedback. The cycle starts with a salinity anomaly and the temperature anomaly set to zero. The sign of the density anomaly is the same as the salinity anomaly because the haline forcing dominates the thermal forcing ($R_\rho < 1$). When the density anomaly is positive (negative), the subsequent anomalous convection brings warm salty (fresh, cold) waters upward and the correlation coefficient c_{TS} between SST and SSS anomalies is then positive. While the growth of salinity variance is controlled only by convection ($S'C'_S > 0$), a competition arises between the restoring surface heat flux and the convection for the growth of temperature variance. When the convection process of the SST anomaly dominates the thermal damping ($-\lambda T'^2 + T'C'_T > 0$), the SST anomalies maintain themselves. The density variance tendency related to air–sea forcing (anomalous restoring heat flux) is positive ($\rho' B' > 0$) because convection strongly and positively correlates SST and SSS anomalies ($c_{TS} > R_\rho$), allowing the initial density perturbation to maintain itself against dissipation.

perturbations (Fig. 7). Furthermore, it appears that the deeper the convection, the higher the temperature and salinity variances related to convective motions. This is the reason why the amplitude of the source term $\rho' B'$ increases eastward and is maximum in the region where the convection is the deepest.

In summary, the interdecadal variability under mixed boundary condition owes its existence to the positive convective surface heat flux feedback in which the positive correlation between temperature (i.e., restoring surface heat flux) and salinity anomalies drives the density variance. The weakness of the density stratification and the increase of the mean temperature and salinity with depth allow the convection to sustain the strong positive correlation between SST and SSS anomalies. A schematic view of this positive feedback is illustrated in Fig. 9.

6. Summary and discussion

Using an idealized geometry flat-bottom ocean model with zero wind forcing and a linearized equation of state, we have pointed out several features that demonstrate the different nature of the interdecadal variability of the thermohaline circulation under mixed boundary conditions (restoring surface temperature and constant freshwater flux) and under constant surface flux for both temperature and salinity (Table 3).

Based on density variance budgets, we have shown that the source of the perturbations differs. Under constant flux boundary conditions (the thermal mode), the source is the downgradient meridional eddy heat fluxes ($-v'T'\partial_y \overline{T}$) in the western boundary current regions as identified earlier by Colin de Verdière and Huck (1999), whereas under mixed boundary conditions (the salinity mode), it is the positive correlation between the SST and SSS anomalies ($\rho_0^2 \alpha\beta\lambda T'S'$) that dominates the density variance tendency. We have demonstrated that these strong correlations are maintained through a positive feedback involving the restoring surface heat flux and the convective adjustment under a particular thermohaline stratification. This may be one of the reasons why the interdecadal variability under mixed boundary conditions has been found to be very sensitive to the convective adjustment scheme in previous works (Weaver and Sarachik 1991b). The positive growth of density variance under mixed boundary conditions requires in addition very special conditions: 1) temperature and salinity must both increase with depth and density stratification must be controlled by salinity, 2) stratification must be sufficiently weak in order that a small positive sea surface density perturbation destabilizes easily the water column, and 3) amplification of SST owing to convective motions must exceed damping through restoring surface heat flux. Such particular conditions should occur mostly at subpolar latitudes of the real ocean rather than at midlatitudes where the stratification is instead controlled by the temperature. It should be stressed that the above requirements are necessary, but not sufficient, conditions to allow decadal variability under mixed boundary conditions; indeed, the small area of net evaporation close to the western edge plays a crucial role as it corresponds to the location where a new cycle emerges (Weaver and Sarachik 1991a,b; Weaver et al. 1993). Additional investigation based on the work of Lenderink and Haarsma (1994) reveals that the net evaporation in this particular region must exceed a low critical value to make the isolated system unstable. The subsequent emerging perturbations are then, eventually, enhanced by the positive convective surface heat flux feedback described in section 5b. The analysis of the vertical structure of perturbations in the most unstable region of the domain has also reveal significant differences between constant flux and mixed boundary conditions. Under constant flux boundary conditions, the density, temperature, and salinity anomalies are well positively

TABLE 3. Summary of the fundamental differences between the interdecadal oscillations under constant air–sea flux (FTFS) and mixed boundary conditions (RTFS).

Expt	FTFS	RTFS
Dominant forcing	Thermal	Haline
Energy source of the oscillation	Downgradient eddy temperature flux: $-\alpha^2 v' T' \partial_y \overline{T}$	Positive correlation between SST′ and SSS′: $\alpha\beta\lambda \mathrm{SST}'\mathrm{SSS}'$
Mechanism	Baroclinic instability in the western boundary region	Positive convective surface heat flux feedback
Mode	Linear	Nonlinear
Role of salinity in the variability	Damping, increasing period	Crucial
Is the convection critical?	No	Yes
Vertical structure of perturbations	Vertical phase lag of quarter period in T', S', ρ'	Dipolar structure of T', no vertical phase lag

correlated at all depths and the lower anomalies lag the upper anomalies by a quarter period. Under mixed boundary conditions, only the temperature anomalies exhibit dipolar structure and no vertical phase lag is observed in any of the tracer fields. In comparison with the purely thermally driven case under constant surface flux, the addition of salinity and constant freshwater flux does not modify the spatial and temporal structures of the perturbations and the mechanism of interdecadal variability, that is, large-scale (generalized) baroclinic instability.

One may object that we have considered some particular experiments in parameter space in order to compare the variability under mixed and flux boundary conditions using the same initial state. A large ensemble of experiments has shown that the parameter range for the existence of oscillations appears to be larger in the case of constant surface fluxes than under mixed boundary conditions. This might be an indication that this latter kind of variability may be less relevant for the real ocean than the former one. However, it is possible that regional interactions between surface heat flux and convective motions give rise to a positive feedback such as that described here under mixed boundary conditions, leading to local generation of perturbations but not necessarily to basinwide decadal variability.

Huck et al. (1999a) carried out an extensive parameter sensitivity analysis of the decadal variability arising under fixed surface fluxes and concluded that the variability is more likely generated by strong circulations associated with large vertical mixing. Using small values of vertical mixing in the upper ocean, such as those estimated by Ledwell et al. (1993) from tracer release experiments in the thermocline, might reduce drastically the growth rate of perturbations. But Huck et al. (1999a) and Huck et al. (2001) have also stressed other important damping sources on the variability, such as horizontal mixing, wind stress forcing, and bottom topography.

The present study is limited to a single-hemisphere basin without the Antarctic Circumpolar Current, which has a large influence on the mean structure of the Atlantic thermohaline circulation (Toggweiler and Samuels 1993; Vallis 2000). However, we believe that our idealized model captures the basic mechanisms of interdecadal variability under mixed and flux boundary conditions. A more realistic geometry would rather modify the structure of the mean circulation and maybe influence the range of parameters for which these oscillations emerge.

The greatest difficulties occur when one attempts to compare results of this kind of variability with observations because of the uncertainty in the parameter range (the strength of turbulent mixing), the long time scales of the processes involved as compared with the period of the most reliable observations, and, in general, the lack of knowledge of the low-frequency variability of the vertical structure of the North Atlantic Ocean. However, as noted earlier by Greatbatch and Zhang (1995), the comparison with realistic models is much easier and the structure of the variability under constant buoyancy flux bears some resemblance with that emerging in more complex climate models (Delworth et al. 1993), with maximum variance in the northwestern part of the Atlantic Ocean. We propose that the investigation of the density variance budget and the structure of perturbations in the more exhaustive climate models should be carried out to identify the unsettled origin of the modes (mixed or flux) that emerge as in Yin and Sarachik (1995) or Delworth et al. (1993) and Delworth and Greatbatch (2000), for instance. Last, the robustness of the interdecadal oscillations under mixed and flux boundary conditions to feedbacks involving the addition of sea ice, wind stress, atmospheric stochastic forcing, or mesoscale turbulence are future studies that might benefit from the viewpoints and methodology developed herein.

Acknowledgments. This work was carried out at Laboratoire de Physique des Océans (UMR 6523 CNRS IFREMER UBO), Université de Bretagne Occidentale, Brest, France. Most of the model integrations have been performed on the Compaq Alpha Server at the numerical computation center of Ifremer (Institut français de recherche pour l'exploitation de la mer, Brest, France).

REFERENCES

Bjerknes, J., 1964: Atlantic air-sea interaction. *Advances in Geophysics*, Vol. 10, Academic Press, 1–82.

Bryan, F., 1986: High-latitude salinity effects and interhemispheric thermohaline circulation. *Nature,* **323,** 301–304.

Chen, F., and M. Ghil, 1995: Interdecadal variability of the thermohaline circulation and high-latitude surface fluxes. *J. Phys. Oceanogr.,* **25,** 2547–2568.

——, and ——, 1996: Interdecadal variability in a hybrid coupled ocean–atmosphere model. *J. Phys. Oceanogr.,* **26,** 1561–1578.

Colin de Verdière, A., 1986: On the mean flow instabilities within the planetary geostrophic equations. *J. Phys. Oceanogr.,* **16,** 1981–1984.

——, 1988: Buoyancy driven planetary flows. *J. Mar. Res.,* **46,** 215–265.

——, and T. Huck, 1999: Baroclinic instability: An oceanic wavemaker for interdecadal variability. *J. Phys. Oceanogr.,* **29,** 893–910.

——, and M. L. Blanc, 2001: Thermal resonance of the atmosphere to SST anomalies. Implications for the Antarctic circumpolar wave. *Tellus,* **53A,** 403–424.

Da Costa, E., and A. Colin de Verdière, 2002: The 7.7y North Atlantic Oscillation. *Quart. J. Roy. Meteor. Soc.,* **128,** 797–817.

Delworth, T. L., and R. J. Greatbatch, 2000: Multidecadal thermohaline circulation variability excited by atmospheric surface flux forcing. *J. Climate,* **13,** 1481–1495.

——, and M. E. Mann, 2000: Observed and simulated multidecadal variability in the northern hemisphere. *Climate Dyn.,* **16,** 661–676.

——, S. Manabe, and R. J. Stouffer, 1993: Interdecadal variations of the thermohaline circulation in a coupled ocean–atmosphere model. *J. Climate,* **6,** 1993–2011.

Deser, C., and M. L. Blackmon, 1993: Surface climate variations over the North Atlantic during winter: 1900–1989. *J. Climate,* **6,** 1743–1753.

Greatbatch, R. J., and S. Zhang, 1995: An interdecadal oscillation in an idealized ocean basin forced by constant heat flux. *J. Climate,* **8,** 81–91.

Haney, R. L., 1971: Surface boundary condition for ocean circulation models. *J. Phys. Oceanogr.,* **1,** 241–248.

Hansen, D. V., and H. F. Bezdek, 1996: On the nature of decadal anomalies in North Atlantic sea surface temperature. *J. Geophys. Res.,* **101,** 8749–8758.

Huang, R. X., and R. L. Chou, 1994: Parameter sensitivity study of the haline circulation. *Climate Dyn.,* **9,** 391–409.

Huck, T., and G. K. Vallis, 2001: Linear stability analysis of the three dimensional thermally-driven ocean circulation: Application to interdecadal oscillations. *Tellus,* **53A,** 526–545.

——, A. Colin de Verdière, and A. Weaver, 1999a: Interdecadal variability of the thermohaline circulation in box-ocean models forced by fixed surface fluxes. *J. Phys. Oceanogr.,* **29,** 865–892.

——, A. J. Weaver, and A. Colin de Verdière, 1999b: On the influence of the parameterization of lateral boundary layers on the thermohaline circulation in coarse resolution ocean-models. *J. Mar. Res.,* **57,** 387–426.

——, G. Vallis, and A. Colin de Verdière, 2001: On the robustness of the interdecadal modes of the thermohaline circulation. *J. Climate,* **14,** 940–963.

Kravtsov, S., and M. Ghil, 2004: Interdecadal variability in a hybrid coupled ocean–atmosphere–sea ice model. *J. Phys. Oceanogr.,* **34,** 1746–1769.

Kushnir, Y., 1994: Interdecadal variations in North Atlantic sea surface temperature and associated atmospheric conditions. *J. Climate,* **7,** 141–157.

Ledwell, J. R., A. J. Watson, and C. S. Law, 1993: Evidence for slow mixing across the pycnocline from an open-ocean tracer-release experiment. *Nature,* **364,** 701–703.

Lenderink, G., and R. J. Haarsma, 1994: Variability and multiple equilibria of the thermohaline circulation associated with deep-water formation. *J. Phys. Oceanogr.,* **24,** 1480–1493.

Levitus, S., 1989: Interpendatal variability of temperature and salinity of intermediate depths of the North Atlantic Ocean, 1970–1974 versus 1955–1959. *J. Geophys. Res.,* **94,** 9679–9685.

Lorenz, E. N., 1955: Available potential energy and the maintenance of the general circulation. *Tellus,* **7,** 157–167.

Mikolajewicz, U., and E. Maier-Reimer, 1990: Internal secular variability in an ocean general circulation model. *Climate Dyn.,* **4,** 145–156.

Munk, W., 1966: Abyssal recipes. *Deep-Sea Res.,* **13,** 707–730.

——, and C. Wunsch, 1998: Abyssal recipes II: Energetics of tidal and wind mixing. *Deep-Sea Res. I,* **45,** 1977–2010.

Pierce, D. W., T. P. Barnett, and U. Mikolajewicz, 1995: Competing roles of heat and freshwater flux in forcing the thermohaline circulation. *J. Phys. Oceanogr.,* **25,** 2046–2064.

Reverdin, G., D. Cayan, and Y. Kushnir, 1997: Decadal variability of hydrography in the upper northern north Atlantic in 1948–1990. *J. Geophys. Res.,* **102,** 8505–8531.

Salmon, R., 1986: A simplified linear ocean circulation theory. *J. Mar. Res.,* **44,** 695–711.

Stern, M. E., 1967: Lateral mixing of water masses. *Deep-Sea Res.,* **14,** 747–753.

Sutton, R. T., and M. R. Allen, 1997: Decadal predictability of north Atlantic sea surface temperature and climate. *Nature,* **388,** 563–567.

te Raa, L. A., and H. A. Dijkstra, 2002: Instability of the thermohaline circulation on interdecadal timescales. *J. Phys. Oceanogr.,* **32,** 138–160.

Toggweiler, J. R., and B. Samuels, 1993: Is the magnitude of the deep-outflow from the Atlantic ocean actually governed by southern hemisphere winds? *The Global Carbon Cycle,* M. Heimann, Ed., NATO ASI Series, Vol. I, Springer, 303–331.

Tziperman, E., J. R. Toggweiler, Y. Feliks, and K. Bryan, 1994: Instability of the thermohaline circulation with respect to mixed boundary conditions: Is it really a problem for realistic models? *J. Phys. Oceanogr.,* **24,** 217–232.

Vallis, G. K., 2000: Large-scale circulation and production of stratification: Effects of wind, geometry, and diffusion. *J. Phys. Oceanogr.,* **30,** 933–954.

Weaver, A. J., and E. S. Sarachik, 1991a: Evidence for decadal variability in an ocean general circulation model: An advective mechanism. *Atmos.–Ocean,* **29,** 197–231.

——, and ——, 1991b: The role of mixed boundary conditions in

numerical models of the ocean's climate. *J. Phys. Oceanogr.,* **21,** 1470–1493.

——, ——, and J. Marotzke, 1991: Freshwater flux forcing of decadal and interdecadal oceanic variability. *Nature,* **353,** 836–838.

——, J. Marotzke, P. F. Cummins, and E. S. Sarachik, 1993: Stability and variability of the thermohaline circulation. *J. Phys. Oceanogr.,* **23,** 39–60.

Welander, P., 1982: A simple heat-salt oscillator. *Dyn. Atmos. Ocean,* **6,** 233–242.

Winton, M., and E. S. Sarachik, 1993: Thermohaline oscillations induced by strong steady salinity forcing of ocean general circulation models. *J. Phys. Oceanogr.,* **23,** 289–304.

Wright, D. G., and T. F. Stocker, 1991: A zonally averaged model for the thermohaline circulation. Part I: Model development and flow dynamics. *J. Phys. Oceanogr.,* **21,** 1713–1724.

Yin, F. L., and E. S. Sarachik, 1995: Interdecadal thermohaline oscillations in a sector ocean general circulation model: Advective and convective processes. *J. Phys. Oceanogr.,* **25,** 2465–2484.